

Simulation of state-dependent high-frequency atmospheric variability associated with ENSO

Jong-Seong Kug · K. P. Sooraj · Daehyun Kim · In-Sik Kang ·
Fei-Fei Jin · Yukari N. Takayabu · Masahide Kimoto

Received: 20 October 2007 / Accepted: 10 June 2008 / Published online: 4 July 2008
© Springer-Verlag 2008

Abstract High-frequency atmospheric variability depends on the phase of El Niño/Southern Oscillation (ENSO). Recently, there is increasing evidence that state-dependent high-frequency atmospheric variability significantly modulates ENSO characteristics. Hence, in this study, we examine the model simulations of high-frequency atmospheric variability and, further, its dependency on the El Niño phase, using atmospheric and coupled GCMs (AGCM and CGCM). We use two versions of physical packages here—with and without convective momentum transport (CMT)—in both models. We found that the CMT simulation gives rise to a large climatological zonal wind difference over the Pacific. Also, both the climate models show a significantly improved performance in simulating the state-dependent noise when the CMT parameterization is implemented. We demonstrate that the better simulation of the state-dependent noise results from a better representation of anomalous, as well as climatological, zonal wind. Our further comparisons between the simulations, demonstrates that low-frequency wind is a crucial factor in determining the state-dependency of high-frequency wind variability. Therefore, it is suggested that

the so-called state-dependent noise is directly induced by the low-frequency wind anomaly, which is caused by SST associated with ENSO.

Keywords ENSO · High-frequency variability · ENSO/MJO interaction · Scale interaction

1 Introduction

The extraordinary westerly wind events (WWEs) in the boreal winter of 1996/1997, which coincided with the onset of the largest El Niño (McPhaden 1999), has led to a number of studies. These studies have mainly suggested the importance of interaction between ENSO and relatively shorter-timescale atmospheric variability such as the Madden and Julian Oscillation (MJO) and WWEs (Moore and Kleeman 1999; Kessler and Kleeman 2000; Vecchi and Harrison 2000; Zhang and Gottschalk 2002; many others). Some of them showed that the enhanced MJO and WWE activities preceded the peak of El Niño by several months (McPhaden 1999; Harrison and Vecchi 1997; Fink and Speth 1997; Zhang and Gottschalk 2002), while others indicated that the MJO and WWEs were led by a large-scale SST anomaly (Luther et al. 1983; Gutzler 1991; Hendon et al. 1999; Vecchi and Harrison 2000; Kessler 2001; Seiki and Takayabu 2007a, b). Recently, Kug et al. (2008b) have shown that the strong activity of short-term atmospheric variability leads an El Niño peak phase by several months over the western Pacific, but is also simultaneously correlated to the ENSO phase over the central Pacific. Also, they have shown that significant correlation is found over most spectral bands of the atmospheric frequency, from synoptic to extended-MJO time scales.

J.-S. Kug (✉) · K. P. Sooraj · D. Kim · I.-S. Kang
Climate Environment System Research Center,
Seoul National University, Seoul 151-742, South Korea
e-mail: kug@hawaii.edu

F.-F. Jin
Department of Meteorology, SOEST, University of Hawaii,
Honolulu, HI, USA

Y. N. Takayabu · M. Kimoto
Center for Climate System Research (CCSR),
University of Tokyo, Tokyo, Japan

The importance of this interaction between two different timescale phenomena is recently supported by several theoretical and modeling studies (Lengaigne et al. 2004; Eisenman et al. 2005; Perez et al. 2005; Zavala-Garay et al. 2005; Jin et al. 2007; Gebbie et al. 2007). In these studies, they did not consider any dependency of high frequency atmospheric variability on the slowly varying large-scale features such as SST. In this paper we will also refer to ‘state-dependent’ noise as a high-frequency (2–90 days) atmospheric variability which depends on a slowly varying low-frequency state. Most previous studies have argued that the interaction between ENSO and the fast atmospheric variability, as modeled by the state-dependent noise forcing or multiplicative noise forcing, modulates not only ENSO instability but also ENSO asymmetry.

The observational, theoretical and modeling studies referred to above indicate that there is a two-way interaction between ENSO-related SST anomaly and atmospheric noise. While the influence of atmospheric noise (e.g. WWE) on the SST anomaly has been investigated in many studies (e.g. Kessler and Kleeman 2000; Gebbie et al. 2007), it is still unclear how the high frequency atmospheric variability is controlled by the ENSO-related SST anomaly and atmospheric low-frequency variability. A sophisticated climate model, embodying most of the dynamical and physical processes, may give a clue to this question. In this context, it is also interesting to check how well state-of-the-art climate models simulate this state-dependent atmospheric noise associated with ENSO. So far, the capability of current state-of-the-art general circulation models (GCMs) to simulate atmospheric noise and its dependency on the ENSO state have not been thoroughly investigated. Therefore, in this study, we will examine the simulations of state-dependent noise in the Seoul National University (SNU) atmospheric GCM (AGCM) and coupled GCM (CGCM) with different physical parameterizations. Hence, here in this study, two kinds of physical packages—with/without convective momentum transport (hereafter CMT)—are implemented for both the models.

Recently, many studies have paid special attention to the parameterization of CMT in order to improve their climate models (Zhang and McFarlane 1995; Gregory et al. 1997; Wu et al. 2003, 2007; Kim et al. 2008). The CMT was often called ‘cumulus friction’ in the earlier studies (Helfand 1979; Thompson and Hartmann 1979). Observational evidence on the importance of the CMT in the momentum budget has also been examined in several works (Stevens 1979; Carr and Bretherton 2001; Tung and Yanai 2002; Lin et al. 2005; Dima et al. 2005). In particular, Kim et al. (2008) showed that the ENSO simulation is significantly improved in the SNU AGCM and CGCM, when CMT parameterization is implemented. They pointed

out that the CMT distinctively changes the pattern and magnitude of the wind anomaly during El Niño periods, which affects not only ENSO amplitude but also the ENSO period. Moreover, we found a striking difference in the high-frequency atmospheric noise between simulations with and without CMT parameterization in both AGCM and CGCM. We investigate these sensitivity experiments for further understanding of the physical dynamics in nature. In addition, we will suggest which factors are crucial in simulating state-dependent noise.

The organization of this paper is as follows. In Sect. 2, the data and the model used are described. Section 3 gives a climatological simulation of high-frequency atmospheric variation in the AGCM and CGCM. The state-dependent noise is compared in several simulations and its relation with low-frequency variation is shown in Sect. 4. The summary and discussion is given in Sect. 5.

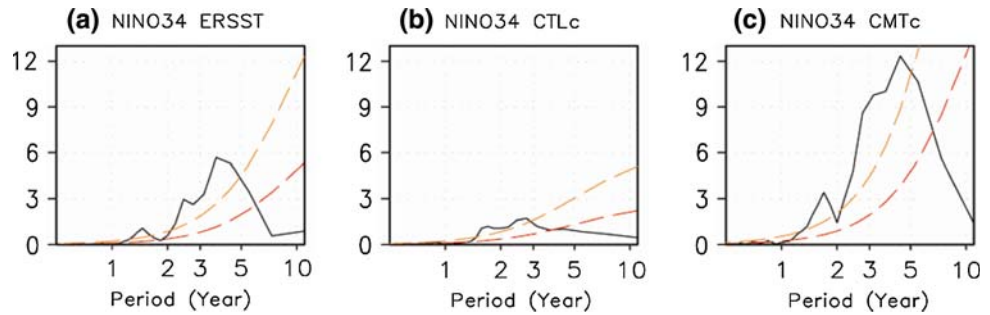
2 Models and data

2.1 Models

The models used in this study are the Seoul National University atmospheric GCM (SNU AGCM) and coupled GCM (SNU CGCM). The SNU AGCM is a global spectral model, with 20 vertical levels in a sigma coordinate. Horizontal resolution T42 version is used. The deep convection scheme is a simplified version of the relaxed Arakawa-Schubert (SAS) scheme (Numaguti et al. 1995). The large-scale condensation scheme consists of a prognostic microphysics parameterization for total cloud liquid water (Le Treut and Li 1991) with a diagnostic cloud fraction parameterization. A non-precipitating shallow convection scheme (Tiedtke 1983) is also implemented in the model for mid-tropospheric moist convection. The boundary layer scheme is a non-local diffusion scheme based on Holtslag and Boville (1993), while the land surface model is from Bonan (1996). The radiation process is parameterized by the two-stream k distribution scheme implemented by Nakajima et al. (1995). Other details of the model physics are described in Lee et al. (2001, 2003).

The CGCM used here was developed at SNU with the same atmospheric component as the AGCM. The oceanic component is the MOM2.2 Oceanic GCM developed at the Geophysical Fluid Dynamics Laboratory (GFDL). The model is a finite difference treatment of the primitive equations of motion using the Boussinesq and hydrostatic approximations in spherical coordinates. The domain of the model covers most global oceans, and its coastline and bottom topography are realistic. The zonal resolution is 1.0° . The meridional grid spacing between 8°S and 8°N is

Fig. 1 Power-spectrum of Nino 3.4 index of **a** ERSST, **b** CTLc and **c** CMTc. Nino 3.4 index is defined as 190°–240°E, 5°S–5°N averaged monthly mean SST anomaly. Dashed lines are representing red noise curve and 90 and 95% confidence level, respectively



1/3°, gradually increasing to 3.0° at 30°S and 30°N, and is fixed at 3.0° in the extratropics. There are 32 vertical levels with 23 levels in the upper 450 m. In the CGCM, a mixed layer model, developed by Noh and Kim (1999) is embedded in the ocean model to improve the climatological vertical structure of the upper ocean. The ocean model communicates once a day with the atmospheric model. The two component models exchange the following data: SST, wind stress, freshwater flux, longwave and shortwave radiation, and turbulent fluxes of sensible and latent heat. Although no flux correction is applied, the model does not exhibit a significant climate drift in the long-term simulation. In addition, the CGCM reasonably simulates the climatology of most oceanic and atmospheric variables. In addition to the climatology, the coupled model reasonably simulates ENSO characteristics, though some systematic bias of ENSO-related patterns is found (Kug et al. 2008a).

In this study, the CMT parameterization suggested by Wu and Yanai (1994), is implemented in AGCM and CGCM. The present parameterization of the CMT was developed based on Eqs. 19 and 20 in Wu and Yanai (1994). Detailed descriptions of the implemented parameterization can be found in Kim et al. (2008).

To examine the impact of the CMT on simulations of ENSO and its state-dependent noise, relatively long simulations of the AGCM and CGCM are used. Two versions of AGCM—with/without CMT—are integrated from 1979 to 1999 with observed SST as a boundary condition. Hereafter, the AGCM simulations with/without CMT parameterization are referred to as CTLa and CMTa, respectively. In addition, the CMT parameterization is implemented in the present coupled GCM. Hereafter, the CGCM simulations with/without CMT are referred to as CTLc and CMTc, respectively. In both simulations, the CGCM is integrated over 200 and 50 years for CTLc and CMTc, respectively. In CTLc, the analysis is done using the last 100 years of data sets. Kim et al. (2008) showed that the climatological bias is significantly improved when the CMT is applied to the present coupled GCM. For example, the cold SST bias and dry precipitation over the central Pacific is reduced by the CMT-induced westerlies and resultant air–sea coupling process.

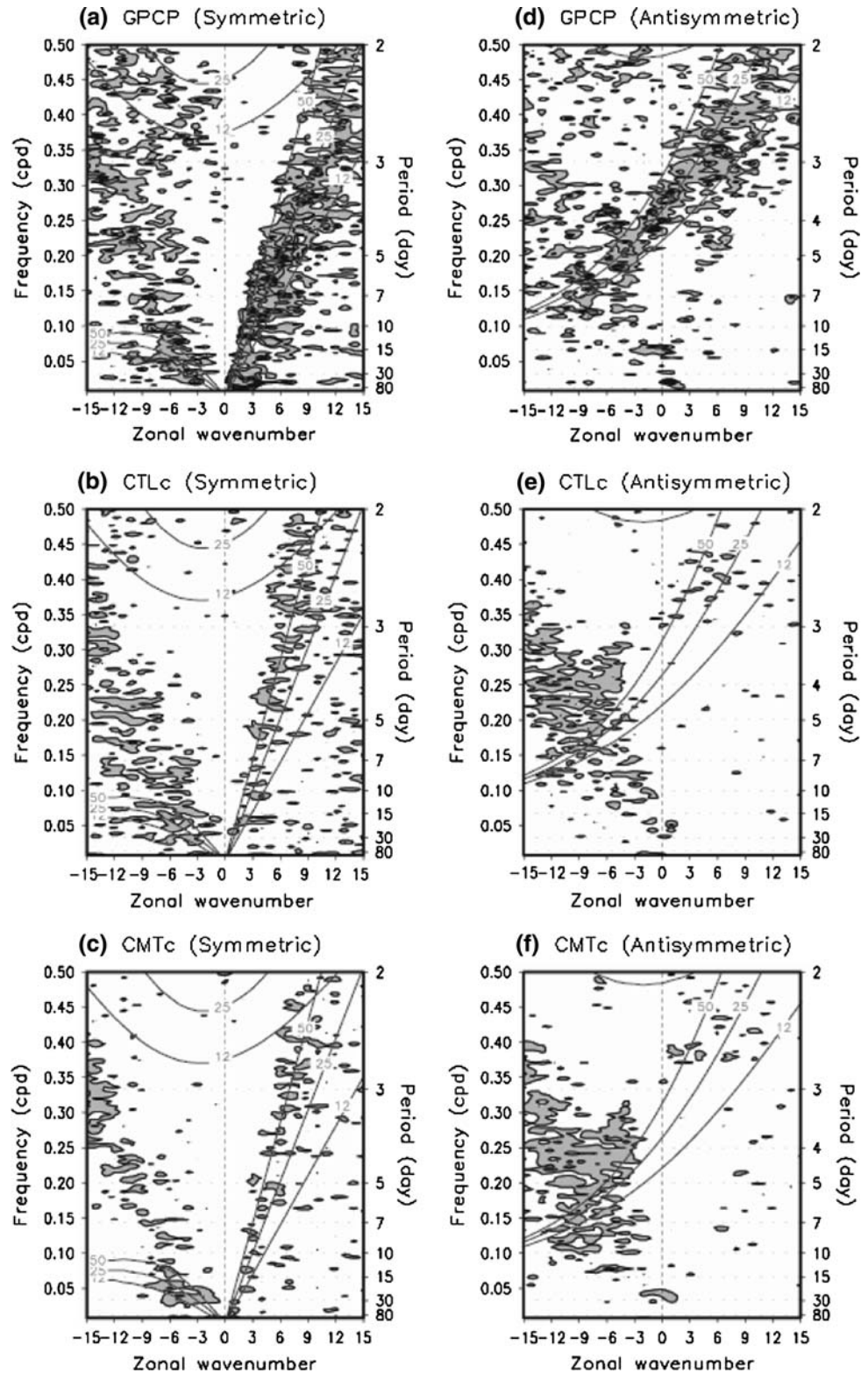
In the following sessions, we will examine the relation between ENSO and high-frequency variability using with and without CMT simulations. Prior to this analysis, it will be worthwhile to comparing the simulations of ENSO and high-frequency variability in both coupled simulations, respectively. Figure 1 shows the power spectra of NINO3.4 SST of observation and two versions of CGCM. We used National Oceanic and Atmospheric Administration (NOAA) Extended Reconstructed Sea Surface Temperature (ERSST 1979–2003) as observation. Observation (black) has broad peak at 2–7 year of period. The CMTc (red) also has broad spectral peak near 4 year while the period of CTLc is shorter than that of observation. In addition, it is quite clear that the CMT parameterization also enhances ENSO variability. The standard deviations of Nino 3.4 index are 0.9 (OBS), 0.7 (CTLc) and 1.4 (CMTc) (see Table 1). Kim et al. (2008) argued that these differences are related to an atmospheric response to the SST forcing, because the CMT parameterization simulates a more realistic low-level wind responses associated with ENSO. The readers are referred to Kim et al. (2008) for further details.

To effectively evaluate and show the realism of atmospheric convection of the coupled models, we followed the method of Wheeler and Kiladis (1999). Figure 2 shows symmetric and antisymmetric raw spectra divided by background spectra. Shaded region means peaks in the individual spectra that are significantly above the background. Because we merely want to show the realism of simulated convective signals, the detailed methods are not described here. The readers are referred to Wheeler and Kiladis (1999). Dispersion curves in the figure represent signals of the Kelvin, equatorial Rossby (ER), and

Table 1 Standard deviation and normalized skewness of NINO3.4 SST in the observational data, CTLc, and CMTc

Expt	Standard deviation	Skewness
OBS	0.9	0.5
CTLc	0.7	−0.3
CMTc	1.4	0.3

Fig. 2 Space–time spectrum precipitation divided by the background spectrum. *Left (Right)* panels are of symmetric (antisymmetric) component of GPCP (*upper*), CTLc (*middle*) and CMTc (*lower*). Superimposed are the dispersion curves of the odd meridional mode numbered equatorial waves for equivalent depths of 12, 25, and 50 m. Frequency spectral width is 1/256 cpd



westward inertio-gravity (WIG) waves in symmetric spectra, of the mixed Rossby-gravity (MRG) and eastward inertia-gravity (EIG) waves in the antisymmetric spectra. There is no much difference between CTLc (Fig. 2b, e) and

CMTc (Fig. 2c, f) with regard to the organization of convection. Both of the simulations have capability to simulate Kelvin, ER and MRG waves with equivalent depth about 50 m. It is deeper than that of observation (25 m, Fig. 2a,

d) and many current coupled climate models show similar discrepancy (Lin et al. 2005). In addition, their relative significance is quite smaller compared to observational one in both simulations. In summary, two versions of the coupled model simulate quite different ENSO characteristics, but similar characteristics of high-frequency atmospheric variability in global sense. Therefore, one may argue the changes of the relation between ENSO and high-frequency variability results from the different characteristics of ENSO simulation. We will discuss this point further in the following sessions.

2.2 Data

The observational data used in this study are SST (monthly means) and zonal winds (daily and monthly means at lower levels) for the period of 1979–1999, same as that of the AGCM simulation period. The monthly mean SST data are from the improved Extended Reconstructed Sea Surface Temperature Version 2 (ERSST.v2) data set (Smith and Reynolds 2004) created by the National Climate Data Center (NCDC).

The daily and monthly wind data are taken from the National Center for Environmental Prediction/National Center for Atmospheric Research (NCEP/NCAR, Kalnay et al. 1996). Daily anomalies are obtained after removing the climatological annual cycle, which is obtained by averaging all the daily data on the same calendar dates. A 2–90 day band-pass LANCZOS filter (using 45 weights, Duchon 1979) is applied to the daily zonal wind anomalies at 925 hPa level, in order to investigate relatively fast atmospheric variability associated with ENSO. We extended the same analysis to the model generated zonal winds and SST. But in the model, we used only wind at 850 hPa, being the lowest available level of atmospheric circulation in the model. Hereafter, the variability of the filtered wind (both in the model and observation) is referred to as atmospheric “noise” for simplicity. The variance of the filtered wind is calculated using a 5 month moving window.

3 Simulation of climatological noise variance

Prior to examining the simulation of state-dependent atmospheric noise, the climatological variance of atmospheric noise is compared in the CTL_a and CMT_a. Figure 3 shows the variance of the filtered 850 hPa zonal wind. The variance is calculated using all seasons during the period of 1979–1999. In both simulations, the variance is relatively large over the western Pacific. In particular, there is a maximum variance over the western north Pacific. In general, the patterns are similar to each other. However, the

overall magnitude of the noise variance is larger in the CMT_a compared to that in CTL_a. The difference is distinctive and its maximum difference is about $10 \text{ m}^2 \text{ s}^{-2}$ over the western Pacific, as shown in Fig. 3c. Compared to the CTL_a, the noise variance is increased by about 60% in CMT_a.

Figure 4 shows the variance of the filtered wind simulated by two coupled GCMs. Compared to the AGCMs, the coupled GCMs simulate relatively weak variance in the high-frequency atmospheric variability. It is possibly related to a cold bias of the coupled GCMs over the tropical Pacific. However, the overall pattern is similar to that of the AGCM simulations. It can be seen that the CMT_c simulates a stronger noise variance than the CTL_c, which is consistent with the case of the AGCM simulations. The difference is relatively large over the western Pacific, and the maximum value is $5 \text{ m}^2 \text{ s}^{-2}$, as shown in Fig. 4c. This indicates that the simulations with CMT parameterization create favorable conditions for stronger activity of short-term atmospheric variability.

How can the CMT parameterization change the short-term atmospheric variability so dramatically? As previous studies pointed out (Stevens 1979; Carr and Bretherton 2001; Tung and Yanai 2002; Lin et al. 2005; Dima et al. 2005), the CMT changes atmospheric circulation by

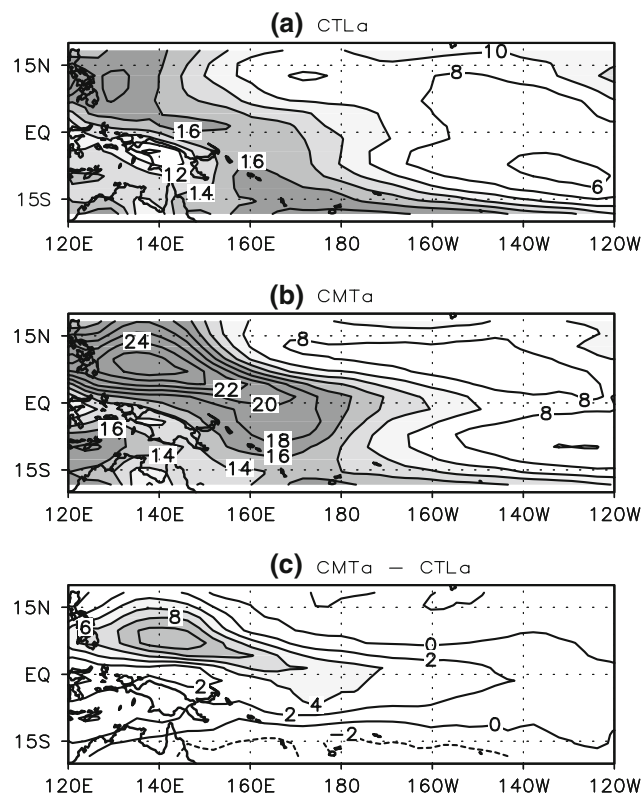


Fig. 3 Variance map of the filtered zonal wind at 850 hPa in **a** CTL_a and **b** CMT_a simulations. **c** Difference between CTL_a and CMT_a

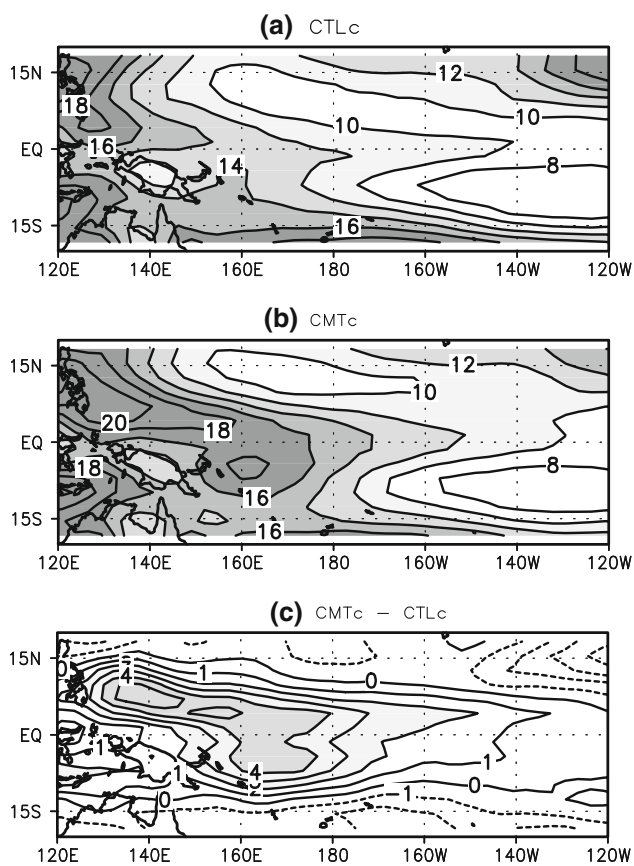


Fig. 4 The same as Fig. 3 except for **a** CTLc and **b** CMTc. **c** Difference between CTLc and CMTc

altering the momentum budget. Kim et al. (2008) also showed, using the present models, that the low-level circulation is changed significantly after the CMT parameterization is implemented to them. Figure 5 shows the climatological difference of zonal wind at 850 hPa from the two AGCM and CGCM simulations. The difference between simulations with and without the CMT clearly shows the westerly wind over most equatorial Pacific regions (Fig. 5a, b). Because climatological westerly vertical shear is overwhelming over the tropical Pacific, it is expected that the CMT increases low-level westerly wind by transporting westerly momentum from the upper atmosphere to the lower atmosphere. A striking difference in the zonal wind appears over the western Pacific. The maximum difference is more than 6 ms^{-1} in both AGCM and CGCM simulations. Moreover it shows an asymmetric pattern, with the maximum differences slightly shifted to the northern hemisphere.

It is interesting to note that the pattern of the climatological wind difference is similar to that of the atmospheric noise variance in both AGCM and CGCM simulations. Therefore, we hypothesize here that the low-level westerly difference produced by the CMT results in significant

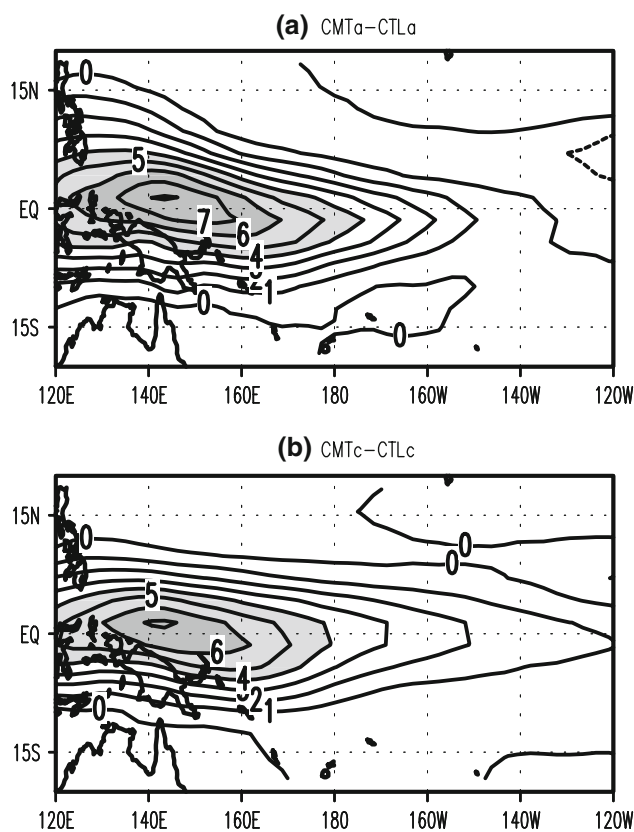
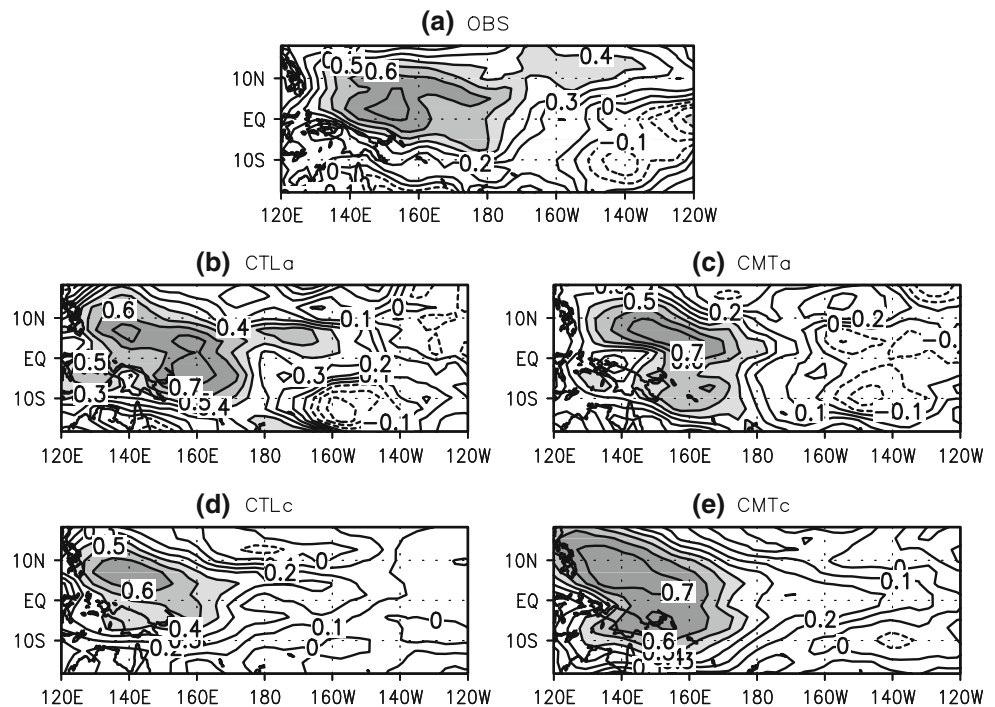


Fig. 5 Difference of the simulated zonal wind climatology at 850 hPa between **a** the CTLa and CMTa, and **b** the CTLc and CMTc

increase in short-term atmospheric variability. Several previous studies partly support our hypothesis. Wang and Xie (1996) showed theoretically that moist atmospheric Rossby waves are strongly excited in the low level under a background easterly vertical shear. Furthermore, recently, Seiki and Takayabu (2007a, b) showed the WWE tends to occur frequently under background low-level westerlies. Also, they showed that the background westerlies create favorable conditions to develop synoptic disturbance by analyzing the kinetic energy budget.

In order to support this hypothesis, we analyzed the observational data and four model simulations further. If the climatological noise variance depends on the climatological zonal wind over the western Pacific, it would be expected that the interannual variation of the noise variance can also be correlated to the interannual variation of the large scale low-level zonal wind circulation. To check this, we defined a western Pacific wind index (WP index), by simply area-averaging the zonal wind over $120^{\circ}\text{--}160^{\circ}\text{E}$, $5^{\circ}\text{S--}5^{\circ}\text{N}$. In order to examine the relation between the WP index and noise variance, we calculated the correlation coefficients not only in the model simulation data but also in the reanalysis data, as shown in Fig. 6. It is clear that the two variables are closely related to each

Fig. 6 Correlation coefficients between WP wind index and variance of the filtered zonal wind in **a** NCEP/NCAR reanalysis data, **b** CTL_a, **c** CMT_a, **d** CTL_c, and **e** CMT_c



other. The correlation coefficients over the western Pacific are more than 0.7 in the reanalysis data and in most simulations. Note that the CMT simulations have a relatively higher correlation coefficient than the others over the western Pacific. However in general, the correlation patterns are broadly similar in the five panels (see Fig. 6), though they have quite different simulations on the low-frequency wind and noise variance. This indicates that this relation is quite robust, regardless of the CMT parameterization, air–sea coupling and climatological basic state. Therefore, these results strongly support our hypothesis that the climatological zonal wind is linked to the difference in simulation of the atmospheric noise variance.

4 Simulation of the state-dependent atmospheric noise associated with ENSO

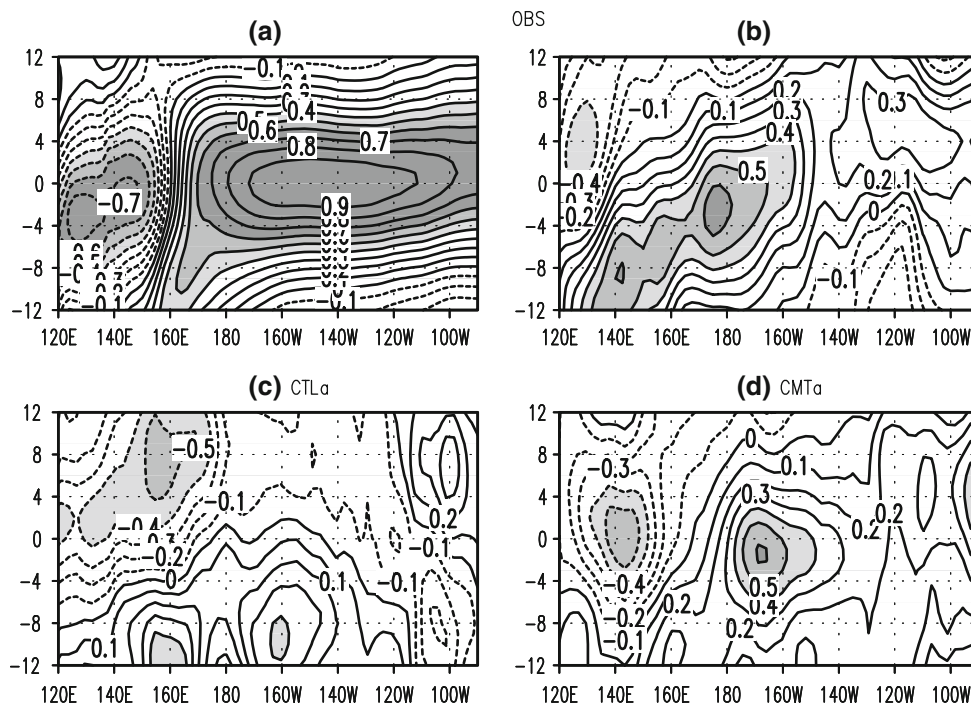
In the previous section, we showed that the present AGCM and CGCM have a large sensitivity to the CMT parameterization in simulating climatological atmospheric noise variance. Also, we showed that atmospheric noise variance is highly dependent on the background wind. It is expected that the interannual relationship of the atmospheric noise to ENSO (i.e. state-dependent noise) will be simulated differently according to the implementation of the CMT parameterization. In this section, we will show firstly the difference in characteristics of the state-dependent noise in the four simulations and then attempt to explain the

contrast in the simulations. Finally, we will revisit our hypothesis suggested in the previous section.

Recently, Kug et al. (2008b) showed that the interannual variability of the atmospheric noise variance is highly dependent on the phase of ENSO by showing a lead-lag correlation between NINO3.4 SST (anomalous SST averaged over 170°–120°W, 5°S–5°N) and the equatorial noise variance. Here, the relationship is reproduced in Fig. 7b. The lead-lag correlations with equatorial SST are also displayed for comparison (Fig. 7a). Though the period for band-pass filtering used in the present study is slightly different from their work, the overall features are mostly identical to their Fig. 1. As shown in Fig. 7b, the enhanced noise variance appears to propagate eastward from the western Pacific at the onset of El Niño to the eastern Pacific during the El Niño decaying period. In particular, stronger (weaker) activities for the atmospheric noise are observed over the western Pacific 7–10 months prior to the mature stage of El Niño (La Niña). The correlation coefficients are more than 0.5 with 99% confidence level. So far, it is not clear why stronger activity in short-term variability, such as WWE and MJO, occurs at that time, which is considered as an important precursor of ENSO onset by some previous studies (Luther et al. 1983; Perigaud and Cassou 2000; Curtis et al. 2004; Lengaigne et al. 2004). We will revisit this point later. In Fig. 7b, a significant negative correlation is also detected over the western Pacific since the peak phase of ENSO.

A distinctive relationship between ENSO and atmospheric noise is found over the central Pacific. The noise

Fig. 7 **a** Lead-lag correlation coefficients between NINO3.4 SST and SST averaged over 5°S–5°N for ERSST. Lead-lag correlation coefficients between NINO3.4 SST and variance of the filtered wind averaged over 5°S–5°N. **b** NCEP/NCAR reanalysis data, **c** CTLa and **d** CMTa. *Y axis* indicates lag months in correlation



variance is simultaneously correlated with the NINO3.4 SST. The correlation coefficients are more than 0.6 with 99% confidence level. This result supports the notion that atmospheric noise depends on the state of ENSO. That is, the El Niño anomaly allows favorable conditions for strong activity of the atmospheric transient zonal wind anomalies in the equatorial Pacific. The state-dependent noise may not only trigger some ENSO events, but also impact the ENSO growth rate and asymmetry (e.g. Jin et al. 2007).

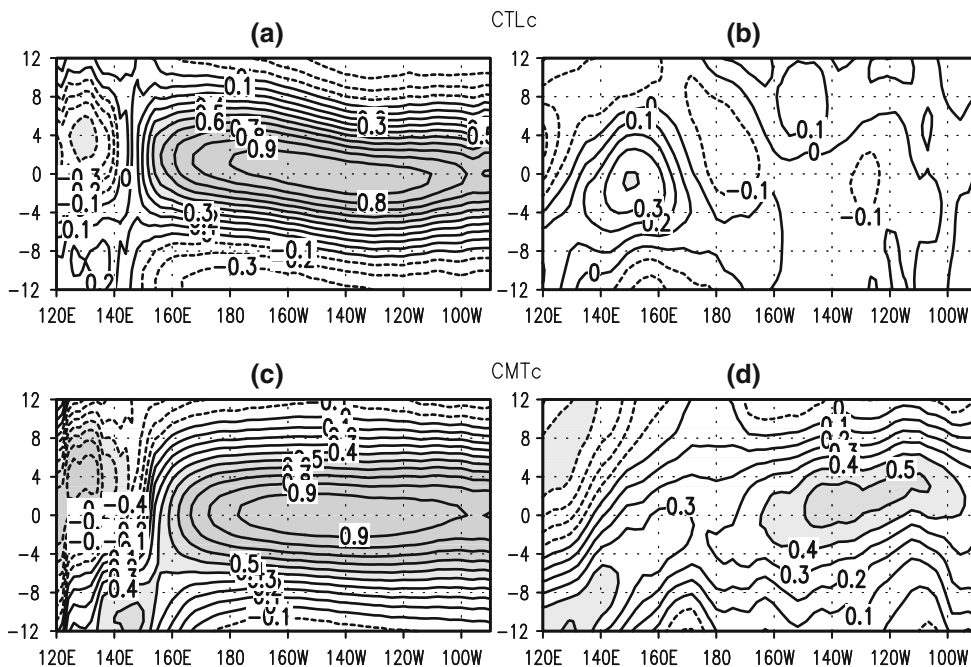
To check whether the present atmospheric model can simulate state-dependent noise, the same analysis is applied to two AGCM simulations (CTLa and CMTa), and two CGCM simulations. As shown in Fig. 7c, the CTLa simulates a weak positive correlation near 160°E, at 12 months prior to the ENSO peak phase, and near 160°W during the most developing period. However, the overall pattern is quite different from the observational one. In particular, the CTLa does not simulate any simultaneous correlation. By contrast, the CMTa (see Fig. 7d) simulates the basic observational feature of the state-dependent noise, though the pattern is shifted by about 20°E. The maximum correlation appears at zero lag, and its value is more than 0.6, as consistent with the observational one. Overall, it seems that the CMTa has better performance than the CTLa, indicating that the CMT parameterization plays a role in simulating the state-dependent noise. It is also quite interesting that both the CMTa and CTLa simulate a positive correlation during the onset phase of ENSO, similar to the observation. Note that both simulations were integrated with the observed SST as a surface boundary

condition. This indicates that the stronger variance is not randomly determined but controlled by a low-frequency signal associated with ENSO. Several previous studies have suggested that the extension of warm pool leads such stronger noise variance (e.g. Kessler et al. 1995; Eisenman et al. 2005; Gebbie et al. 2007). However, we will suggest later that the low-frequency wind is responsible for the strong noise variance during the onset phase of ENSO.

Figure 8 shows simulations of the SST and state-dependent noise in the present two versions of the CGCM. In the CTLc, weak positive correlation at lag zero is confined over 140°–160°E, as shown Fig. 8b. Also, the CTLc does not have positive correlation during the onset phase or negative correlation during decaying phase within the Pacific basin. However, the CMTc exhibits better agreement with observational correlation pattern (see Fig. 8d). It simulates a significant correlation during the mature phase, though the location of maximum correlation is shifted to the east. Also, the CMTc shows a positive correlation during the onset phase and a negative correlation during decaying phase in the western Pacific. In summary, both the AGCM and CGCM with CMT parameterization simulate state-dependent noise better than those without CMT parameterization. This implies that the CMT plays a significant role in simulating the state-dependent noise associated with ENSO in both AGCM and CGCM.

Now, two critical questions can be raised based on the above results. How does CMT parameterization alter the simulation of state-dependent noise? What dynamical process controls the noise variance during the onset phase

Fig. 8 Lead-lag correlation of NINO3.4 SST onto **a** CTLc SST averaged over 5°S–5°N and **b** CTLc variance of the filtered wind averaged over 5°S–5°N. In **(c, d)**, same as that of **(a, b)** but for CMTc



when the SST signal is weak? To address these questions, low-level wind associated with ENSO is analyzed in the two CMT simulations, which have better performance in terms of the state-dependent noise.

Figure 9 shows the lead-lag correlation and regression coefficients between NINO3.4 SST and equatorial zonal wind at 850 hPa. The equatorial wind is averaged over 5°S–5°N. In the observation (Fig. 9a), the westerly wind anomaly propagates eastward from the western Pacific to the eastern Pacific during the El Niño developing period. Note that there is a westerly anomaly over the western Pacific, at 12 months prior to the peak time of El Niño, when the SST signal is weak there. Kug et al. (2005) pointed out that the westerly anomaly is linked to the Indian Ocean SST, so that it plays a role in initiating the onset of El Niño. As shown in the previous section, the noise variance is correlated well to the low-level wind in this region. Thus, this implies that a stronger noise at the onset phase is related to the anomalous westerlies.

The anomalous westerlies move to the eastern Pacific after the peak phase of El Niño. Thus, the western Pacific wind changes from an anomalous westerly at the onset phase to easterlies at the peak phase. It is quite interesting that atmospheric noise over the western Pacific consistently changes from strong activity to weak activity. Furthermore, as the anomalous westerlies propagate eastward, the strong noise variance also moves eastward (see Figs. 7a, 9a), indicating that the low-level wind is a crucial component in controlling atmospheric short-term variability.

As shown in Fig. 9, both the AGCM and CGCM simulate the relation between NINO3.4 SST and the equatorial

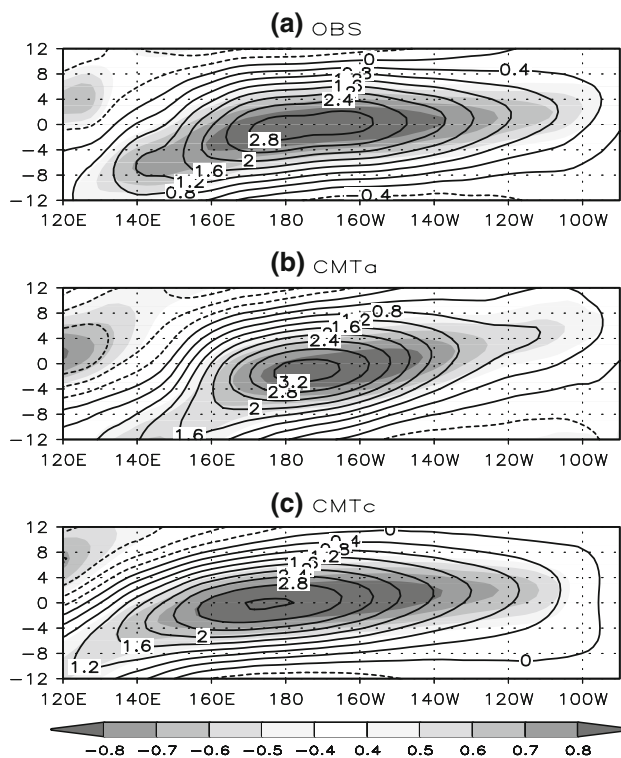


Fig. 9 Lead-lag correlation (Shaded) and regression (Contour) coefficients between NINO3.4 SST and zonal wind at 850 hPa averaged 5°S–5°N. **a** NCEP/NCAR reanalysis data, **b** CMTa and **c** CMTc. Y axis indicates lag months in correlation

zonal wind very well. However, some differences between the simulation and observation are found. In the AGCM, the WP westerly at the onset phase is slightly shifted to the east. The WP easterly at the peak phase is also shifted to

the east. According to the location of the zonal wind, the noise variance is also shifted to the east during the corresponding phase, as shown in Fig. 7c. On the other hand, the CMTc simulates the westerly wind too far to the west during the onset phase. Also, the zonal wind at the peak phase is elongated too far eastward compared to the observational phase. These differences of zonal wind are also consistent with those of the noise variance in the CMTc simulation (Fig. 8b). These results support the view once again that the noise variance is strongly dependent on the low-level wind.

Kim et al. (2008) showed using the present AGCM that the simulation of the El Niño-related wind anomaly is significantly improved when the CMT parameterization is implemented. They also showed that the present CGCM with the CMT simulates better anomalous westerlies over the central Pacific, while the CGCM without the CMT simulates anomalous westerlies which are too weak and shifted toward the western Pacific. Without the CMT, both AGCM and CGCM simulate a relatively weak wind anomaly, as shown in Kim et al. (2008). Also, when the CMT is not used, the regression coefficients over the central Pacific are reduced by about 40 and 50% in AGCM and CGCM, respectively. This may explain why the CTLa and CTLc perform poorly in the simulation of the state-dependent noise, as shown in Figs. 5, 6.

So far, we have shown that the low-level zonal wind is clearly related to the state-dependent noise. In the conventional view, the state-dependent noise tends to be considered as a SST-dependent noise such as NINO3.4 SST (Jin et al. 2007; Kug et al. 2008b) and warm pool extension (Eisenman et al. 2005; Gebbie et al. 2007). Hence, it will be interesting here to examine which variable, SST or zonal wind, affects the short-term atmospheric variation more effectively, though they are correlated well to each other. To test this, a CP wind index is defined as simply area-averaging over the NINO4 region (150°E–150°W, 5°S–5°N), which represents the ENSO-related large scale wind circulation. Figures 10 and 11 show the lag-lead correlation between the CP wind index and the noise variance. It is seen that the overall pattern is similar to the case of NINO3.4 SST (see Figs. 7, 8), because the CP wind index is highly correlated to the NINO3.4 SST. However, the correlation coefficients are increased at zero lag, not only in the observation but also in the four simulations when the CP wind index is used.

To show this more clearly, the partial correlation is calculated by excluding the effects of the NINO3.4 SST and CP wind index, respectively. The partial correlation (Cohen and Cohen 1983) is calculated by linearly removing the effect of the other index. Recently, this method has been frequently used in climate studies, (e.g. Kug and Kang 2006). Figure 12 shows the partial correlation in the

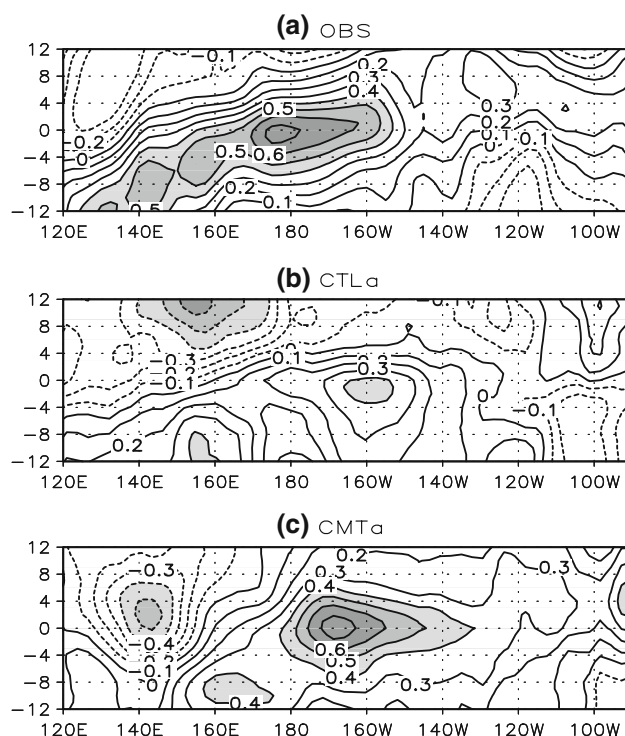


Fig. 10 Lead-lag correlation coefficients between CP wind index and variance of the filtered wind averaged over 5°S–5°N. **a** NCEP/NCAR reanalysis data, **b** CTLa and CMTa. *Y* axis indicates lag months in correlation

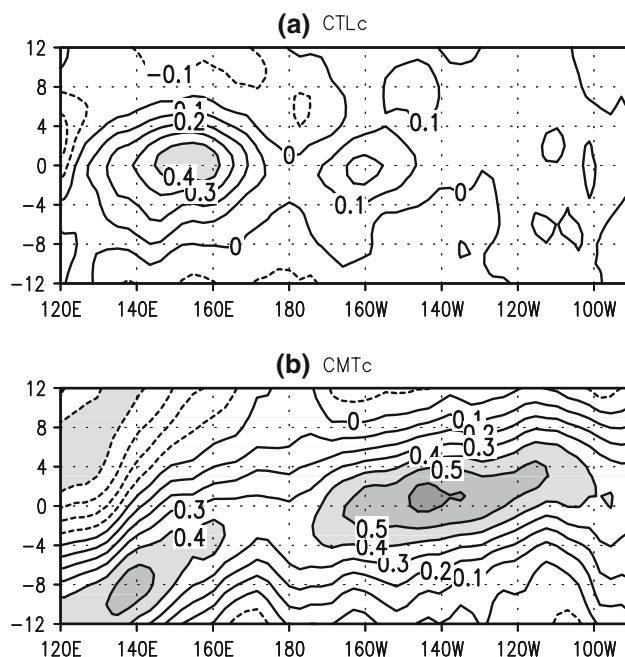


Fig. 11 The same as Fig. 10 except for **a** CTLc and **b** CMTc

observation and four simulations. When the effect of the CP wind index is linearly removed, the partial correlation between NINO3.4 SST and atmospheric noise variance

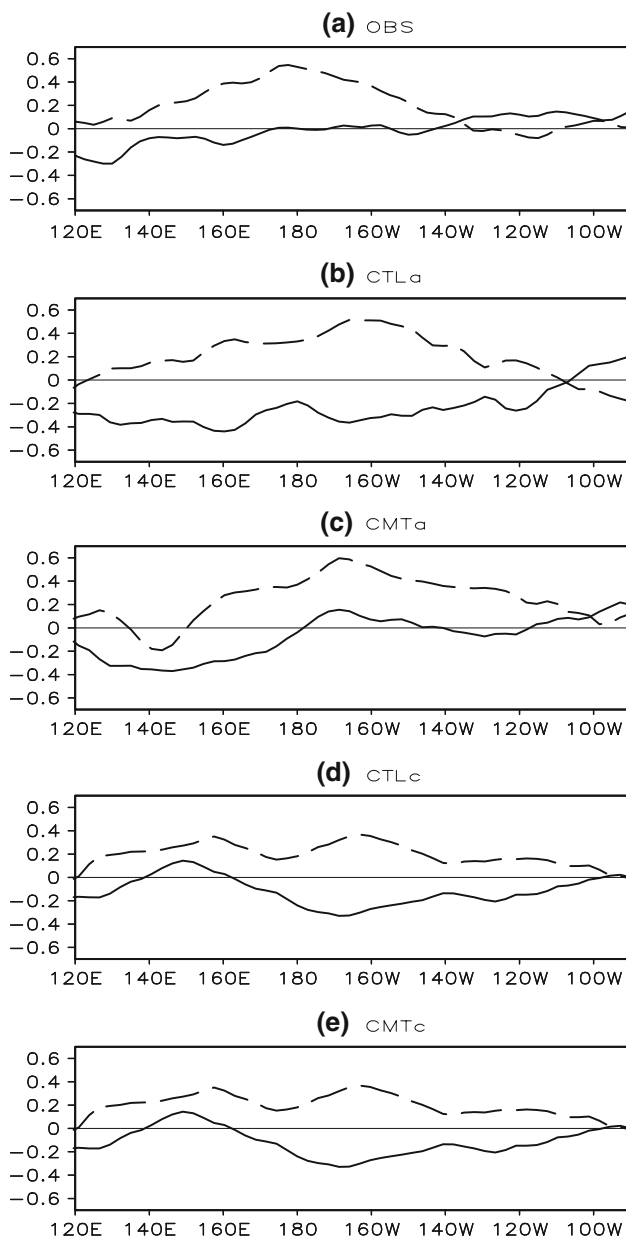


Fig. 12 Partial correlation of NINO3.4 SST (*solid line*) and CP wind index (*dashed line*) with the variance of the filtered zonal wind averaged over 5°S–5°N after the effect of CP wind index (for *solid line*) and NINO3.4 SST (for *dashed line*) is removed, in the **a** observational data, **b** CTL α , **c** CMT α , **d** CTL c and **e** CMT c , respectively

shows a weaker correlation in the observation as well as in all four simulations. On the other hand, when the effect of NINO3.4 SST is removed, the CP wind index has a stronger correlation with the atmospheric noise variance over the central Pacific, though the correlation coefficient is slightly reduced compared to those of Figs. 10 and 11. This indicates that the atmospheric noise variance is more directly related to low frequency wind anomaly. Therefore, the so-called state-dependent noise is directly induced by

the low-frequency wind anomaly, which is caused by SST associated with ENSO.

5 Summary and discussion

The state-dependent atmospheric noise associated with ENSO is examined using climate model simulations. We found that the AGCM and CGCM exhibit significantly improved performance in simulating the state-dependent noise when CMT parameterization is implemented. This implies that the state-of-the-art climate model has an ability to simulate state-dependent noise. A better simulation of state-dependent noise results from better representation of the anomalous zonal wind as well as the climatological wind. Based on these results, we may say that the state-dependent noise associated with ENSO can be considered as a wind-dependent noise rather than a SST-dependent noise.

The present CMT c simulates a stronger state-dependent atmospheric noise compared to the CTL c . Thus, it will be quite interesting to compare ENSO characteristics between the two simulations. This gives us a chance to examine theoretical works on the role of the state-dependent noise (or multiplicative noise). After the CMT parameterization is implemented, the standard deviation as well as the skewness of NINO3.4 SST is increased significantly (see Fig. 1; Table 1). Kim et al. (2008) argued that the increased ENSO variability results from better simulation of the westerly anomaly associated with El Niño over the central Pacific. Because the CMT c simulates a stronger westerly anomaly, the ENSO variability increases. However at this stage, we cannot rule out other possible mechanisms, which may also change these ENSO characteristics. Based on theoretical work, Jin et al. (2007) pointed out that the state-dependent noise increases ENSO instability and ENSO skewness. Their argument is consistent with the observed change in our model simulations. Thus, it is possible that a stronger state-dependent noise may partly contribute to the change of ENSO magnitude and skewness. More careful examination is needed in further studies.

Our results have interesting implications for the onset of El Niño by creating a link between the two schools of thoughts. Both of them, respectively, showed the importance of (a) short-term atmospheric variability (Luther et al. 1983; Perigaud and Cassou 2000; Curtis et al. 2004; Lengaigne et al. 2004) and (b) anomalous westerlies (Weisberg and Wang 1997; Kug et al. 2005) to the onset of El Niño. The former group argued that short-term variability plays a role in triggering the onset of El Niño events while the latter emphasized a role for the WP anomalous westerlies. Based on our results, the stronger noise and

anomalous westerly wind are closely correlated to each other. Furthermore, our results show that stronger variance during the onset phase is systematically determined, because the AGCM with prescribed SST captures the relationship well. In short, anomalous westerlies with stronger noise activity can be good precursor for the onset of El Niño.

We showed here the clear statistical relationships between low-frequency zonal wind variation and activity of high-frequency atmospheric variation, both in observational and model-simulated data. However, it is not still clear how the low-frequency zonal wind can affect high-frequency atmospheric variability. Though the present study is not intended to elucidate the dynamical processes involved in this scale interaction, we suggest a possible explanation.

Recently, Seiki and Takayabu (2007b) suggested a mechanism of synoptic-scale eddy development in the generation of WWEs over the western and central Pacific under low-frequency environmental westerlies. They argued that the dominant contribution to eddy kinetic energy (EKE) is a barotropic energy conversion term, which is related to the zonal convergence of the environmental zonal wind (du/dx). The low-frequency environmental westerlies centered near the equator provide strong zonal convergence and meridional shear, resulting in favorable conditions for synoptic eddy development. The synoptic eddies grow through barotropic conversion from the mean flow during the westerly MJO periods. Therefore, they argued that the WWEs frequently occur in the westerly phase of MJO as well as in the El Niño phase. This indicates that WWEs are also state-dependent on the MJO phase (c.f. Maloney and Hartmann 2000, 2001).

On the other hand, the dependency of WWEs on the MJO phase can amplify MJO activity. The westerly (easterly) phase of MJO is accompanied by a strong (weak) activity of synoptic disturbance, as we discussed. If the system is purely linear, the activity of the synoptic disturbance cannot affect MJO variation, having a relatively longer time scale. However, precipitation variability, closely related to wind variability, is highly nonlinear—and always positive. Thus, the strong activity of synoptic disturbance results in more precipitation in the MJO time scale, because of the nonlinearity of precipitation. Accordingly, the state-dependent WWEs can lead to more precipitation in the westerly phase, and less precipitation in the easterly phase. This means that MJO activity is increased by interaction between phenomena with different time scales, indicating WWE–MJO interaction.

The existence of this WWE–MJO interaction has an important implication for ENSO. It is well known that the ENSO system largely controls low-frequency wind vari-

ability over the tropical Pacific. During El Niño onset and peak phases, the anomalous westerlies intensify the WWE–MJO interaction over the western-central Pacific. This indicates that both WWE and MJO activity are intensified under the El-Niño related background westerlies. This is a possible dynamical reason for the association of the state-dependent noise with El Niño. Kug et al. (2008b) showed using observational data that a significant correlation between NINO3.4 and noise variance appears over most frequencies of atmospheric variability, from the synoptic scale to the extended MJO scale (see their Fig. 2). This partly supports the existence of the WWE–MJO interaction and its relation to ENSO. For further understanding of ENSO, the detailed dynamics behind the interactions between multi-time scale phenomena (e.g. WWE, MJO and ENSO) should be elucidated, and this will be a big challenge to future studies.

We have shown in this study that the low-frequency westerlies create favorable conditions for strong noise variance using observational and model data. Though here we established a clear statistical relationship with possible physical explanations, they are subjected to the limitation of statistical analysis. This is because the statistical analysis hardly tells causation for the strong relation. For example, one may argue that the stronger atmospheric noise may intensify the low-frequency westerlies. Hence, it may be difficult to draw conclusion, solely based on statistical analysis. To clearly separate the influence of the low-frequency wind on the high-frequency variability, further studies, based on experimental modeling, may be required. In this regard, Sooraj et al. (2008) recently carried out numerical experiment to show how the low-frequency wind controls the high-frequency atmospheric variability. They clearly showed the response of the large scale circulation to generate high-frequency variability, thus supporting our argument well.

However, it is also possible that there is two-way feedback between low-frequency wind and high-frequency wind variability. This means that the high-frequency variability, modulated by the low-frequency circulation, may affect the low-frequency through a feedback loop. It is well known that the short-term variability is highly skewed to the westerly phase. While WWEs are observed frequently, EWEs (Easterly Wind Events) are only rarely observed. This skewed high-frequency atmospheric variability may change the low-frequency variability of atmospheric circulation by its residual contribution. This indicates a positive feedback between the phenomena of two different timescales. This interaction will have tremendous implications for ENSO and MJO dynamics. Hence the present paper opens a new avenue for exploring further studies, of course with more detailed dynamics.

Acknowledgments This work was mostly done when J.-S. Kug visited CCSR during the summer in 2007. This work was supported by the Korea Meteorological Administration Research and Development Program under Grant CATER_2006-4206 and the second stage of the Brain Korea 21 Project. F.-F. Jin was partly supported by NSF grants ATM-0652145 and ATM-0650552 and NOAA grants GC01-229. M. Kimoto was supported by the Innovative Program of Climate Change Projection for the 21st Century (KAKUSHIN program) of the Ministry of Education, Culture, Sports, Science, and Technology (MEXT) in Japan. Y. Takayabu is partially supported by the Global Environment Research Fund (S-5-2) of the Ministry of the Environment, Japan.

References

- Bonan GB (1996) A land surface model (LSM version 1.0) for ecological, hydrological, and atmospheric studies: technical description and user's guide. NCAR Tech. Note NCAR/TN-417 + STR, Natl Cent For Atmos Res, Boulder, Colorado, pp 150
- Carr MT, Bretherton CS (2001) Convective momentum transport over the tropical Pacific: budget estimates. *J Atmos Sci* 58:1673–1693
- Cohen J, Cohen P (1983) Applied multi regression/correlation analysis for behavioral sciences. Lawrence Erlbaum Associate, Hillsdale, p 545
- Curtis S, Adler RF, Huffman GJ, Gu G (2004) Westerly wind events and a precipitation in the eastern Indian Ocean as predictors for El Niño: climatology and case study for the 2002–2003 El Niño. *J Geophys Res* 109:D20104. doi:10.1029/2004JD004663
- Dima IM, Wallace JM, Kraucunas I (2005) Tropical zonal momentum balance in the NCEP reanalyses. *J Atmos Sci* 62:2499–2513
- Duchon C (1979) Lancos filtering in one and two dimensions. *J Appl Meteorol* 18:1016–1022
- Eisenman I, Yu L, Tziperman E (2005) Westerly wind bursts: ENSO's tail rather than the dog? *J Clim* 18:5224–5238
- Fink A, Speth P (1997) Some potential forcing mechanisms of the year-to-year variability of the tropical convection and its intraseasonal (25–70 day) variability. *Int J Climatol* 17:1513–1534
- Gebbie G, Eisenman I, Wittenberg A, Tziperman E (2007) Modulation of westerly wind bursts by sea surface temperature: a semi-stochastic feedback for ENSO. *J Atmos Sci* (in press)
- Gregory D, Kershaw R, Inness PM (1997) Parameterization of momentum transport by convection.2. Tests in single-column and general circulation models. *Q J R Meteorol Soc* 123:1153–1183
- Gutzler DS (1991) Interannual fluctuations of intraseasonal variance of near-equatorial winds. *J Geophys Res* 96:3173–3185
- Harrison DE, Vecchi GA (1997) Westerly wind events on the tropical Pacific, 1986–95. *J Clim* 10:3131–3156
- Helfand HM (1979) Effect of cumulus friction on the simulation of the January Hadley circulation by the Glas model of the general-circulation. *J Atmos Sci* 36:1827–1843
- Hendon H, Zhang C, Glick J (1999) Interannual variation of the Madden-Julian oscillation during austral summer. *J Clim* 12:2538–2550
- Holtlag AAM, Boville BA (1993) Local versus nonlocal boundary layer diffusion in a global climate model. *J Clim* 6:1825–1842
- Jin F-F, Lin L, Timmermann A, Zhao J (2007) Ensemble-mean dynamics of the ENSO recharge oscillator under state-dependent stochastic forcing. *Geophys Res Lett* 34:L03807. doi:10.1029/2006GL027372
- Kalnay E et al (1996) The NCEP/NCAR 40-year reanalysis project. *Bull Am Met Soc* 77:437–471
- Kessler W (2001) EOF representations of the Madden-Julian oscillation and its connection with ENSO. *J Clim* 14:3055–3061
- Kessler WS, Kleeman R (2000) Rectification of the Madden-Julian oscillation into the ENSO cycle. *J Clim* 13:3560–3575
- Kessler WS, McPhaden MJ, Weickmann KM (1995) Forcing of intraseasonal Kelvin waves in the equatorial Pacific. *J Geophys Res* 100:10613–10631
- Kim D, Kug J-S, Kang I-S, Jin F-F, Wittenberg AT (2008) Tropical Pacific impacts of convective momentum transport in the SNU coupled GCM. *Clim Dyn*. doi:10.1007/s00382-007-0348-4
- Kug J-S, Kang I-S (2006) Interactive feedback between ENSO and the Indian Ocean. *J Clim* 19:1784–1801
- Kug J-S, An S-I, Jin F-F, Kang I-S (2005) Preconditions for El Niño and La Niña onsets and their relation to the Indian Ocean. *Geophys Res Lett* 32:L05706. doi:10.1029/2004GL021674
- Kug J-S, Kang I-S, Choi D-H (2008a) Seasonal climate predictability with tier-one and tier-two prediction systems. *Clim Dyn*. doi:10.1007/s00382-007-0264-7
- Kug J-S, Jin F-F, Sooraj KP, Kang I-S (2008b) Evidence of the state-dependent atmospheric noise associated with ENSO. *Geophys Res Lett* 35:L05701. doi:10.1029/2007GL032017
- Le Treut H, Li Z-X (1991) Sensitivity of an atmospheric general circulation model to prescribed SST changes: feedback effects associated with the simulation of cloud optical properties. *Clim Dyn* 5:175–187
- Lee M-I, Kang I-S, Kim J-K, Mapes BE (2001) Influence of cloud-radiation interaction on simulating tropical intraseasonal oscillation with an atmospheric general circulation model. *J Geophys Res* 106:14219–14233
- Lee M-I, Kang I-S, Mapes BE (2003) Impacts of cumulus convection parameterization on aqua-planet AGCM simulations of tropical intraseasonal variability. *J Meteorol Soc Jpn* 81:963–992
- Lengaigne M, Guilyardi E, Boulanger JP, Menkes C, Delecluse P, Inness P, Cole J, Slingo J (2004) Triggering of El Niño by westerly wind events in a coupled general circulation model. *Clim Dyn* 23:601–620
- Lin JL, Zhang MH, Mapes B (2005) Zonal momentum budget of the Madden-Julian oscillation: the source and strength of equivalent linear damping. *J Atmos Sci* 62:2172–2188
- Luther DS, Harrison DE, Knox RA (1983) Zonal winds in the central equatorial Pacific and El Niño. *Science* 222:327–330
- Maloney ED, Hartmann DL (2000) Modulation of Eastern North Pacific hurricanes by the Madden-Julian oscillation. *J Clim* 13:1451–1460
- Maloney ED, Hartmann DL (2001) The Madden-Julian oscillation, barotropic dynamics, and north Pacific tropical cyclone formation. Part I: observation. *J Atmos Sci* 58:2545–2558
- McPhaden MJ (1999) Genesis and evolution of the 1997–1998 El Niño. *Science* 283:950–954
- Moore A, Kleeman R (1999) The non-normal nature of El Niño and intraseasonal variability. *J Clim* 12:2965–2982
- Nakajima T, Tsukamoto M, Tsushima Y, Numaguti A (1995) Modelling of the radiative processes in an AGCM. In: Matsuno T (ed) *Climate system dynamics and modelling*, vol I-3. University of Tokyo, Tokyo, pp 104–123
- Noh Y, Kim HJ (1999) Simulations of temperature and turbulence structure of the oceanic boundary layer with the improved near-surface process. *J Geophys Res Oceans* 104:15621–15634
- Numaguti A, Takahashi M, Nakajima T, Sumi A (1995) Development of an atmospheric general circulation model. In: Matsuno T (ed) *Climate system dynamics and modelling*, vol I-3. University of Tokyo, Tokyo, pp 1–27
- Perez CL, Moore AM, Zavaly-Garay J, Kleeman R (2005) A comparison of the influence of additive and multiplicative stochastic forcing on a coupled model of ENSO. *J Clim* 18:5066–5085

- Perigaud C, Cassou C (2000) Importance of oceanic decadal trends and westerly wind bursts for forecasting El Niño. *Geophys Res Lett* 27(3):389–392
- Seiki A, Takayabu YN (2007a) Westerly wind bursts and their relationship with intraseasonal variations and ENSO. Part I: statistics. *Mon Weather Rev* 135:3325–3345
- Seiki A, Takayabu YN (2007b) Westerly wind bursts and their relationship with intraseasonal variations and ENSO. Part II: energetics over the Western and Central Pacific. *Mon Wea Rev* 135:3346–3361
- Smith TM, Reynolds RW (2004) Improved extended reconstruction of SST (1854–1997). *J Clim* 17:2466–2477
- Sooraj KP, Kim D, Kug J-S, Yeh S-W, Jin F-F, Kang I-S (2008) Effects of the low frequency zonal wind variation on the high-frequency atmospheric variability over the tropics. Submitted to *Clim Dyn*
- Stevens DE (1979) Vorticity, momentum and divergence budgets of synoptic-scale wave disturbances in the tropical eastern Atlantic. *Mon Weather Rev* 107:535–550
- Thompson SL, Hartmann DL (1979) Cumulus friction-estimated influence on the tropical mean meridional circulation. *J Atmos Sci* 36:2022–2026
- Tiedtke M (1983) The sensitivity of the time-mean large-scale flow to cumulus convection in the ECMWF model. Workshop on convection in large-scale numerical models. ECMWF, 28 Nov–1 Dec 1983, pp 297–316
- Tung WW, Yanai M (2002) Convective momentum transport observed during the TOGA COARE IOP. Part I: general features. *J Atmos Sci* 59:1857–1871
- Vecchi GA, Harrison DE (2000) Tropical Pacific sea surface temperature anomalies, El Niño and equatorial westerly events. *J Clim* 13:1814–1830
- Wang B, Xie X (1996) Low-frequency equatorial waves in vertically sheared zonal flow. Part I: stable waves. *J Atmos Sci* 53:449–467
- Weisberg RH, Wang C (1997) Slow variability in the equatorial west-central Pacific in relation to ENSO. *J Clim* 10:1998–2017
- Wheeler M, Kiladis GN (1999) Convectively-coupled equatorial waves: analysis of clouds and temperature in the wavenumber-frequency domain. *J Atmos Sci* 56:374–399
- Wu XQ, Yanai M (1994) Effects of vertical wind shear on the cumulus transport of momentum—observations and parameterization. *J Atmos Sci* 51:1640–1660
- Wu XQ, Liang XZ, Zhang GJ (2003) Seasonal migration of ITCZ precipitation across the equator: why can't GCMs simulate it? *Geophys Res Lett* 30(15):1824. doi:[10.1029/2003GL017198](https://doi.org/10.1029/2003GL017198), 2003
- Wu XQ, Deng L, Song X, Zhang GJ (2007) Coupling of convective momentum transport with convective heating in global climate simulations. *J Atmos Sci* 64:1334–1349
- Zavala-Garay J, Zhang C, Moore A, Kleeman R (2005) The linear response of ENSO to the Madden–Julian oscillation. *J Clim* 18:2441–2459
- Zhang Q, Gottschalk J (2002) SST anomalies of ENSO and the Madden–Julian oscillation in the equatorial Pacific. *J Clim* 15:2429–2445
- Zhang GJ, Mcfarlane NA (1995) Role of convective scale momentum transport in climate simulation. *J Geophys Res* 100:1417–1426